Pergamon

J. Mech. Phys. Solids, Vol. 44, No. 11, pp. 1799–1830, 1996

0022–5096/96 $15.00 + 0.00

PII: S0022–5096(96)00055–5

DYNAMIC CRACK PROPAGATION IN PIEZOELECTRIC MATERIALS—PART I. ELECTRODE SOLUTION

SHAOFAN LI

Department of Mechanical Engineering, Northwestern University, Evanston, Illinois, U.S.A.

PETER A. MATAGA†

Software Production Research Department, Bell Laboratories, Naperville, Illinois, U.S.A.

(*Received* 13 *March* 1995; *in revised form* 19 *March* 1996)

ABSTRACT

An analysis is performed for the transient response of a semi-infinite, anti-plane crack propagating in a hexagonal piezoelectric medium. The mixed boundary value problem is solved by transform methods together with the Wiener–Hopf and Cagniard–de Hoop techniques. As a special case, a closed form solution is obtained for constant speed crack propagation under external anti-plane shear loading with the conducting electrode type of electric boundary condition imposed on the crack surface (a second type of boundary condition is considered in Part II of this work).

In purely elastic, transversely isotropic elastic solids, there is no antiplane mode surface wave. However, for certain orientations of piezoelectric materials, a surface wave will occur—the Bleustein–Gulyaev wave. Since surface wave speeds strongly influence crack propagation, the nature of antiplane dynamic fracture in piezoelectric materials is fundamentally different from that in purely elastic solids, exhibiting many features only associated with the in-plane modes in the elastic case.

For a general distribution of crack face tractions, the dynamic stress intensity factor and the dynamic electric displacement intensity factor are derived and discussed in detail for the electrode case. As for in-plane elastodynamic fracture, the stress intensity factor and energy release rate go to zero as the crack propagation velocity approaches the surface wave speed. However, the electric displacement intensity does not vanish. Copyright © 1996 Elsevier Science Ltd

Keywords: A. crack propagation and arrest, A. dynamic fracture, A. electromechanical process, B. piezoelectric material, C. piezoelectric effect.

1. INTRODUCTION

More than a century has passed since the brothers Curie discovered the piezoelectric effect in 1880 (Cagniard, 1939). Today, over a hundred piezoelectric materials or composites are known (Pohanka and Smith, 1988). Due to their intrinsic electromechanical coupling behaviors, piezoelectric materials, particularly piezoelectric ceramics, have been widely used for applications such as sensors, filters, ultrasonic generators and actuators.

More recently, due to emergence of piezoelectric composites, the use of piezoelectric

† Part of this work was carried out while the author was a member of the Department of Aerospace Engineering, Mechanics & Engineering Science, University of Florida, U.S.A.

materials has gone beyond the traditional application domain of small electric devices. Since Bailey and Hubbard's pioneer work (Bailey and Hubbard, 1985), piezoelectric materials have been employed as integrated active structural elements. These adaptive structures are capable of monitoring and adapting to their environment, providing a "smart" response to the external conditions. The interested reader is referred to a state of art survey by Rao and Sunar (1994).

In some of these applications, a major concern in practical operations has been mechanical failure of the piezoelectric layers and the interface to the bulk material. Fracture on the macro- and the micro-scale can lead to undesirable mechanical and dielectric responses for these advanced materials. The fracture process for piezoelectric materials is thus of some practical interest, and has recently been the subject of active research. Parton (1976, 1988) and Deeg (1980) appear to have been the first to conduct systematic theoretical research in this area, while the last decade has seen many contributions, such as McMeeking (1989a, b, 1990), Li *et al.* (1990), Pak (1990, 1992a, b), Sosa (1990, 1991, 1992), Suo *et al.* (1992), Wang (1992), Zhang *et al.* (1992) and Maugin (1993, 1994).

The main results that appear in the literature to date can be summarized as follows:

—In a homogeneous piezoelectric material, the stress and induced electric fields exhibit $r^{-1/2}$ singularity in the vicinity of the crack tip. [For interface cracks, the situation is complex, in more ways than one (Suo *et al.*, 1992).]
—Electric fields may promote or retard crack propagation.

This literature focuses almost entirely on the static electro-mechanical analysis; much less attention has been paid to dynamic crack problems. However, there are strong reasons to anticipate that piezoelectric behavior will strongly affect dynamic crack growth, because of some well-known phenomena in surface wave propagation.

Piezoelectricity enables the existence of certain kinds of bound surface wave. For instance, in piezoelectric materials with a symmetry of class $C_{6v}(\equiv 6mm)$, an acoustic surface wave—the Bleustein–Gulyaev wave—may occur if one chooses the sixfold axis c normal to its sagittal plane (Bleustein, 1968; Gulyaev, 1969). This SH mode surface wave has deeper penetrating length and lower energy loss than does a Rayleigh wave (Maugin, 1983); therefore, it is not only easily excited, but also easily detected. It is thus of fundamental importance in the related wave scattering and inverse scattering problems in piezoelectric materials. Since dynamic crack extension is a process of crack surface growth, we expect surface wave characteristics to be intrinsically linked to crack behavior, as is the case in the purely elastodynamic case for the in-plane modes of crack growth.

In this paper, we explore the anti-plane dynamic growing crack problem. Owing to its mathematical simplicity, the problem of anti-plane dynamic propagation in an elastic medium can be solved in an exact and elementary manner. However, as a benchmark problem of dynamic fracture mechanics, the elastic anti-plane problem is lacking a physical "obligatory sophistication", because no anti-plane mode surface wave exists. In contrast, the anti-plane piezoelectric problem provides both mathematical simplicity and interesting physics. This combination of utilitarian and aesthetic appeal echoes Viktorov's comment on the discovery of the Bleustein–Gulyaev wave: "[it] adds a flavor of elegance to the family of surface waves" (Viktorov, 1981).

Specifically, the motion of a semi-infinite, anti-plane moving crack in an unbounded 6*mm* piezoelectric medium is studied for the case where a concentrated point load is applied on the crack surfaces. On the line ahead of the crack tip, the fundamental solutions are obtained in an explicit manner, so that the intensity factors are derived for the general distribution of applied stress loading. However, the problem is made more complex than the corresponding elastodynamic case by the variety possible in the electrical conditions on the newly created crack faces.

From the surface wave standpoint, there exist two kinds of Bleustein Gulyaev wave: one compatible with an "electrode" boundary condition, the other with a "vacuum abutted" boundary condition. In the fracture mechanics literature, previous work has been considered "conducting" and "insulating" crack (Suo, 1993), but the influence of this distinction on the dynamic behavior has not been investigated. As we will show in this paper and its sequel, the boundary conditions necessitate somewhat different treatments of the problem.

In this paper, we consider the "electrode" case, for which the crack faces are assumed to be conducting and grounded. As will be seen, the solution presented here may be interpreted more broadly than just as being a particular model of a "conducting crack". The "vacuum" case, where the crack is assumed to contain an impermeable medium, is considered in Part II of this work.

While not as rich as the vacuum case, the electrode case has some interesting features. When the crack propagation speed is below the "electrode" Bleustein–Gulyaev wave velocity

$$c_{\mathrm{bg}} = \sqrt{\frac{\bar{c}_{44}}{\rho}}\sqrt{1-k_e^4},$$

the asymptotic behavior of the field variables is similar to that of static fracture solutions, which exhibit $r^{-1/2}$ singularity for both stress and electric displacement. The dynamic stress intensity factor, however, goes to zero when the crack speed approaches c_{bg} in contrast to the anti-plane elastodynamic case, where the dynamic stress intensity factor goes to zero only at the longitudinal shear wave speed. Curiously, however, the dynamic intensity factor for electric displacement does not vanish at the Bleustein–Gulyaev wave speed.

2. FORMULATION OF THE PROBLEM

2.1. *Governing equations*

The body of literature concerning the mechanics of piezoelectric materials is enormous; it suffices to refer to a few influential works (Cady, 1946; Berlincourt *et al.*, 1964; Tiersten, 1969; Auld, 1973). Here the notation of Tiersten (1969) is followed to write the governing equations for linear piezoelectric materials as follows:

—equations of motion

$$\sigma_{ij,i} = \rho\ddot{u}_j; \tag{1}$$

—electrostatic charge conservation

$$D_{i,i} = 0; \tag{2}$$

—strain–displacement relations

$$\varepsilon_{ij} = \tfrac{1}{2}(u_{i,j} + u_{j,i}); \tag{3}$$

—electric field–electric potential relations

$$E_k = -\phi_{,k}; \tag{4}$$

—linear, piezoelectric constitutive relations

$$\sigma_{ij} = c^E_{ijkl}\varepsilon_{kl} - e_{kij}E_k, \tag{5}$$

$$D_i = e_{ikl}\varepsilon_{kl} + \varepsilon^S_{ik}E_k, \tag{6}$$

where c^E_{ijkl} are the elastic moduli, e_{kij} are the piezoelectricity coefficients, and ε^S_{ij} are the dielectric permittivities (with the superscript E or S indicating material constants measured under conditions of constant electric field or constant strain, respectively);
—mechanical boundary conditions

$$\sigma_{ij}n_j = T_i \quad \text{on } S_\sigma; \quad u_i = \bar{u}_i \quad \text{on } S_u; \tag{7}$$

—electrical boundary conditions

$$D_i n_i = -q_s \quad \text{on } S_D \quad \phi = \bar{\phi} \quad \text{on } S_\phi, \tag{8}$$

where S_σ, S_u and S_D, S_ϕ identify appropriate subsets of the domain boundary.

In this paper, attention is focused on the class of piezoelectric materials with hexagonal symmetry (6*mm*). Materials of this symmetry class (single crystal or poled polycrystals) have been used for many different industrial purposes, PZT ceramics for example, because of their high piezoelectric coupling coefficients.

Let X, Y and Z denote regular Cartesian coordinates, where the Z-axis orients in the direction of the sixfold axis of a piezoelectric crystal or in the poling direction of a poled piezoelectric composite. The governing equations simplify considerably if we are only interested in the out-of-plane displacement component and the in-plane electric field components, i.e.

$$u_X = u_Y = 0, \quad u_Z = w(X, Y, t), \tag{9}$$

$$E_X = E_X(X, Y, t), \quad E_Y = E_Y(X, Y, t), \quad E_Z = 0. \tag{10}$$

Switching from tensor to Voigt notation (Parton and Kudryatvsev, 1988), the simplified governing equations have the form

$$c^E_{44}\nabla^2 w + e_{15}\nabla^2\phi = \rho\ddot{w}, \tag{11}$$

$$e_{15}\nabla^2 w - \varepsilon^S_{11}\nabla^2\phi = 0, \tag{12}$$

where ∇^2 is the two-dimensional Laplacian operator, $\nabla^2 \triangleq (\partial^2/\partial X^2) + (\partial^2/\partial Y^2)$; ρ is the mass density; c^E_{44}, e_{15} and ε^S_{11} are elastic, piezoelectric and dielectric constants, respec-

tively, and the superposed dot indicates material differentiation with respect to time. In what follows, we shall drop the superscript E and S, if no confusion is caused thereby. For easy reference, the nontrivial constitutive equations are

$$\sigma_{XZ} = c_{44}\frac{\partial w}{\partial X} + e_{15}\frac{\partial \phi}{\partial X}, \tag{13}$$

$$\sigma_{YZ} = c_{44}\frac{\partial w}{\partial Y} + e_{15}\frac{\partial \phi}{\partial Y}, \tag{14}$$

$$D_X = e_{15}\frac{\partial w}{\partial X} - \varepsilon_{11}\frac{\partial \phi}{\partial X}, \tag{15}$$

$$D_Y = e_{15}\frac{\partial w}{\partial Y} - \varepsilon_{11}\frac{\partial \phi}{\partial Y}. \tag{16}$$

Following Bleustein (1968), a new function ψ is introduced as

$$\psi \triangleq \phi - \frac{e_{15}}{\varepsilon_{11}} w. \tag{17}$$

By substituting (17) into (11) and (12), the system of equations is transformed into the canonical form

$$\nabla^2 w = \frac{\rho}{\bar{c}_{44}}\ddot{w}, \tag{18}$$

$$\nabla^2 \psi = 0, \tag{19}$$

where

$$\bar{c}_{44} \triangleq c_{44}^E + \frac{e_{15}^2}{\varepsilon_{11}^S} \tag{20}$$

is the piezoelectrically stiffened elastic constant.

In terms of independent variables w and ψ, the constitutive equations (13)–(16) can be rewritten as follows

$$\sigma_{XZ} = \bar{c}_{44}\frac{\partial w}{\partial X} + e_{15}\frac{\partial \psi}{\partial X}, \tag{21}$$

$$\sigma_{YZ} = \bar{c}_{44}\frac{\partial w}{\partial Y} + e_{15}\frac{\partial \psi}{\partial Y}, \tag{22}$$

$$D_X = -\varepsilon_{11}\frac{\partial \psi}{\partial X}, \tag{23}$$

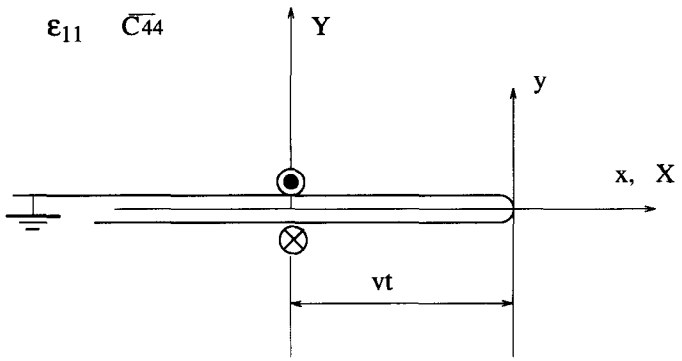

Fig. 1. The running crack subjected to concentrated point load.

$$D_Y = -\varepsilon_{11}\frac{\partial \psi}{\partial Y}. \tag{24}$$

2.2. *Semi-infinite moving crack*

Consider a semi-infinite crack located at $Y = 0$, $X < 0$ in an unbounded piezoelectric body (Fig. 1). It is assumed that the crack is in a static equilibrium state when $t < 0$ and its leading edge is parallel to the poling direction of the piezoelectric body. At $t = 0^+$, a pair of concentrated longitudinal shear forces is applied on the surface of the pre-existing semi-infinite crack and then the crack is assumed to propagate at a constant speed v.

For dynamic fracture problems, it is usually convenient to study the crack propagation in a moving coordinate system (x, y, z), with

$$x = X - vt, \quad y = Y, \quad z = Z. \tag{25}$$

In addition, we define the nondimensional parameter

$$s \triangleq (1 - v^2/c^2)^{1/2}, \tag{26}$$

where

$$c \triangleq (\bar{c}_{44}/\rho)^{1/2} \tag{27}$$

is the speed of the piezoelectrically stiffened bulk shear wave.

By making use of (25), the equations of motion in the moving coordinate system are cast into the form

$$s^2\frac{\partial^2 w}{\partial x^2} + \frac{\partial^2 w}{\partial y^2} + \frac{2v}{c^2}\frac{\partial^2 w}{\partial x\,\partial t} - \frac{1}{c^2}\frac{\partial^2 w}{\partial t^2} = 0, \tag{28}$$

$$\frac{\partial^2 \psi}{\partial x^2} + \frac{\partial^2 \psi}{\partial y^2} = 0. \tag{29}$$

As is customary in linear transient crack growth problems (Freund, 1990), we investigate the perturbation solution corresponding to transient loading of the existing and

newly created crack faces, under the assumption that the pre-existing state is quiescent and can be removed by superposition. For such a solution, the remote boundary condition may be taken as

$$\left.\begin{aligned}\sigma_{yz}(x,y,t) &= 0\\ D_y(x,y,t) &= 0\end{aligned}\right\} \quad |y| \to \infty. \tag{30}$$

Though different in origin, these conditions play a similar role to a wave radiation condition.

Following the approach introduced by Freund (1972a), we take as the fundamental problem that of a concentrated crack face load with transient crack growth, so that the following mechanical boundary conditions are imposed

$$\begin{cases} \sigma_{yz}(x,0,t) = -\delta(x+vt)H(t) & x < 0 \qquad (31a)\\ w(x,0,t) = 0 & x \geqslant 0 \qquad (31b)\end{cases}$$

where the antisymmetry of the loading and initial conditions has been used to introduce the second condition.

In a purely elastic solid, the exact solution of the above problem may be straightforwardly obtained (Ma and Chen, 1992). The piezoelectric case is more complicated, with most of the difficulty stemming from the imposition of the electrical boundary conditions.

2.3. *Electrical boundary conditions*

The issue of how to impose the electrical boundary conditions along the crack surfaces in piezoelectric fracture modeling is a controversial one (Suo *et al.*, 1992; Pak, 1990). The difficulty is due both to the diversity of physical reality and to mathematical complications. McMeeking (1989b) has noted in the context of purely electrical loading that:

> If a closed slit is cut into a homogeneous dielectric, the opposing surfaces are still in contact. Consequently, the material is effectively seamless as far as an electrostatic field is concerned and the field will not be perturbed by the presence of the crack. Exceptions arise when the crack behaves as a conducting surface or is filled with a vanishingly thin medium which is impermeable to the electric field.

So far, several electric boundary conditions on the crack surface have been proposed:

—effectively seamless slit (Parton, 1976): $\phi^+ = \phi^-$, $D_n^+ = D_n^-$;
—impermeable void (Li *et al.*, 1990; Pak, 1990): $D_n^+ = D_n^- = 0$;
—crack filled with conducting fluid (McMeeking, 1989a, b): $\phi^+ = \phi^-$.

Each of these assumptions provide useful analytical simplification, though there is not general agreement on their physical reasonableness, particularly in the case of a static finite crack. Moreover, these conditions appear to exclude some of the surface wave phenomena examined in our work, in particular those discussed in the vacuum

boundary condition case. Here we consider boundary conditions of the type dealt with in the electroacoustic literature (Bleustein, 1968; Gulyaev, 1969; Auld, 1973).

Two kinds of electric surface conditions are usually considered. In the first case, the crack surface is assumed to be covered with a thin metal film with infinite conductivity, which shorts out the horizontal component of **E** at the crack surface but does not affect the mechanical boundary conditions. This metallized interpretation, which was elaborated by Bleustein (1968), is equivalent to assuming that the crack surfaces are coated with an infinitesimally thin, perfectly conducting electrode that is grounded, i.e.

$$\phi(x, 0^+, t) = \phi(x, 0^-, t) = 0 \quad -\infty < x < 0. \tag{32}$$

Although this metallic coating condition is chiefly a mathematically convenient proposition, it offers a good approximation for many electroacoustic problems and has become a standard benchmark problem (Auld, 1973). Moreover, this situation actually exists, if there is a thin conducting film embedded in the middle of the piezoelectric body and a crack propagates along this interface, as might occur in piezoelectric composite layer structures. This boundary condition is also appropriate if the crack surfaces are in a state of electrical contact, or if the crack is filled with conducting gas or liquid.

The full set of boundary conditions for the electrode case considered in this paper can be summarized as

$$\sigma_{yz}(x, 0, t) = -\delta(x+vt)H(t), \quad x < 0, \tag{33}$$

$$w(x, 0, t) = 0, \quad x \geqslant 0, \tag{34}$$

$$\phi(x, 0, t) = \frac{e_{15}}{\varepsilon_{11}} w(x, 0, t) + \psi(x, 0, t) = 0, \quad -\infty < x < 0, \tag{35}$$

with quiescent initial conditions

$$w(x, y, 0) = 0, \quad \dot{w}(x, y, 0) = 0, \tag{36}$$

$$\psi(x, y, 0) = 0, \quad \dot{\psi}(x, y, 0) = 0. \tag{37}$$

Note that because of the antisymmetry of the problem, it will also be true that ϕ vanishes on the line ahead of the crack.

For the second kind of electric field boundary conditions (the "vacuum" case), the void formed by an opening crack is assumed to be a vacuum region. Therefore, there is no free charge around the surfaces of cracks, but there will be a nonzero potential $\tilde{\phi}$ in the vacuum region. The extent to which this is appropriate has been discussed in the finite crack case, but is likely to be a good approximation to reality in the long crack case, since the relative permittivity of air is close to 1.

From a mathematical point of view, the solution procedure becomes more complicated in this case, since the equations must be solved in multiple regions—the piezoelectric region and the vacuum region—which interact at the crack surface. (Furthermore, external electric loading may be applied to the crack surfaces under the second type of boundary conditions.) The two cases have significantly different

characteristics with respect to dynamic energy release rate, as is discussed in Part II of this work. For the moment, we proceed with the simpler case.

3. INTEGRAL EQUATION SOLUTIONS

3.1. *Transform methods*

In this section, the standard procedure of multiple Laplace transforms is employed to derive the solutions of the above mixed initial-boundary value problem. The multiple transforms are introduced for the variable pair (x, t). To suppress the time variable t, the usual, one-sided Laplace transform is applied

$$f^*(x,y,p) = \int_0^\infty f(x,y,t)\exp(-pt)\,\mathrm{d}t, \tag{38}$$

$$f(x,y,t) = \frac{1}{2\pi\mathrm{i}}\int_{Br_1} f^*(x,y,p)\exp(pt)\,\mathrm{d}p, \tag{39}$$

where the inversion integration is taken over the usual Bromwich path.

To suppress the spatial variable x, the two-sides Laplace transform is used

$$\hat{f}^*(\zeta,y,p) = \int_{-\infty}^\infty f^*(x,y,p)\exp(-p\zeta x)\,\mathrm{d}x, \tag{40}$$

$$f^*(x,y,p) = \frac{p}{2\pi\mathrm{i}}\int_{Br_2} \hat{f}^*(\zeta,y,p)\exp(p\zeta x)\,\mathrm{d}\zeta. \tag{41}$$

After transformation, the governing equations (28) and (29) become

$$\left[\frac{\mathrm{d}^2}{\mathrm{d}y^2} - p^2\left(\frac{1}{c^2} - 2\frac{v}{c^2}\zeta - s^2\zeta^2\right)\right]\hat{w}^*(\zeta,y,p) = 0, \tag{42}$$

$$\left[\frac{\mathrm{d}^2}{\mathrm{d}y^2} - p^2(\varepsilon^2 - \zeta^2)\right]\hat{\psi}^*(\zeta,y,p) = 0. \tag{43}$$

Consideration of the boundary conditions at infinity and of the problem's anti-symmetry suggests choosing solutions of the form

$$\hat{w}^*(\zeta,y,p) = \begin{cases} \dfrac{1}{p^m}A(\zeta)\exp(-p\alpha y) & y > 0 \\ -\dfrac{1}{p^m}A(\zeta)\exp(p\alpha y) & y < 0. \end{cases} \tag{44}$$

$$\hat{\psi}^*(\zeta, y, p) = \begin{cases} \dfrac{1}{p^m} B(\zeta) \exp(-p\beta y) & y > 0 \\ -\dfrac{1}{p^m} B(\zeta) \exp(p\beta y) & y < 0. \end{cases} \tag{45}$$

The concentrated loading boundary condition dictates the choice $m = 2$, and the coefficient functions α and β may be written as

$$\alpha(\zeta) \triangleq \sqrt{\frac{1}{c^2} - \frac{2v\zeta}{c^2} - s^2\zeta^2} = s\sqrt{\left(\zeta + \frac{1}{c-v}\right)\left(\frac{1}{c+v} - \zeta\right)}, \tag{46}$$

$$\beta(\zeta) \triangleq \lim_{\varepsilon \to 0} \sqrt{\varepsilon^2 - \zeta^2}. \tag{47}$$

Here ε is introduced as an auxiliary (positive real) perturbation parameter, with the understanding that whenever ε is present, the final expressions involved are always evaluated at $\varepsilon = 0$ at the end of the manipulation.

Remark 1. The technique of introducing an auxiliary parameter has been widely used in applying transform methods to solve partial differential equations (there are many useful examples in Duffy's book (1994)). In particular, Broberg (1973) used the approach to facilitate the Wiener–Hopf decomposition that arose in his analysis of elastoplasto-dynamic crack growth.

However, one may in fact motivate the "trick" for our present application by careful consideration of the quasi-static approximation implicit in the original governing equations. The basic hypotheses of the quasi-static approximation (Auld, 1973) are: first, the rotational electric field can be neglected; second, all the electromechanical wave solutions travel at velocities compared to which the speed of electromagnetic waves, c_l, is very large. From this point of view, it is physically plausible to write (43) as

$$\left[\frac{\mathrm{d}^2}{\mathrm{d}y^2} - p^2(\varepsilon^2 - \zeta^2)\right]\bar{\psi}^*(\zeta, y, p) = 0, \tag{48}$$

where ε is of order $\mathcal{O}(1/c_l)$. A detailed account from this perspective of the electromagneto-elastic equations in linear piezoelectric materials and the related SH mode electromagnetoacoustic surface wave has been carried out recently by one of the authors (Li, 1996); by taking into account the full Maxwell equations, a generalized wave speed equation for SH mode electromagnetoacoustic surface wave is derived, which reduces to Bleustein–Gulyaev wave when $c/c_l \to 0$.

In (44) and (45), $\mathrm{Re}(\alpha(\zeta), \beta(\zeta)) \geqslant 0$ in the plane with branch cuts

$$\alpha: \quad \mathrm{Im}(\zeta) = 0 \quad \mathrm{Re}(\zeta) < -1/(c-v), \quad \text{and} \quad \mathrm{Re}(\theta) > 1/(c+v), \tag{49}$$

$$\beta: \quad \mathrm{Im}(\zeta) = 0 \quad \mathrm{Re}(\zeta) < -\varepsilon, \quad \text{and} \quad \mathrm{Re}(\zeta) > \varepsilon. \tag{50}$$

From the transformed electric boundary condition

$$\phi^*(x,0,p) = \frac{e_{15}}{\varepsilon_{11}} w^*(x,0,p) + \psi^*(x,0,p)$$
$$= \frac{1}{2\pi i p} \int_{\zeta_\beta - i\infty}^{\zeta_\beta + i\infty} \left(\frac{e_{15}}{\varepsilon_{11}} A(\zeta) + B(\zeta) \right) d\zeta$$
$$= 0, \quad -\infty < x < 0, \tag{51}$$

it follows that

$$B(\zeta) = -\frac{e_{15}}{\varepsilon_{11}} A(\zeta). \tag{52}$$

Defining

$$k_e^2 \triangleq \frac{e_{15}^2}{\varepsilon_{11} \bar{c}_{44}}, \tag{53}$$

the integral representations (for $y > 0$) can be expressed in terms of a single unknown function

$$\sigma_{xz}^*(x,y,p) = \frac{\bar{c}_{44}}{2\pi i} \left(\int_{\zeta_\alpha - i\infty}^{\zeta_\alpha + i\infty} \zeta A(\zeta) \exp(-p(\alpha y - \zeta x))\, d\zeta \right.$$
$$\left. - k_e^2 \int_{\zeta_\beta - i\infty}^{\zeta_\beta + i\infty} \zeta A(\zeta) \exp(-p(\beta y - \zeta x))\, d\zeta \right), \tag{54}$$

$$\sigma_{yz}^*(x,y,p) = -\frac{\bar{c}_{44}}{2\pi i} \left(\int_{\zeta_\alpha - i\infty}^{\zeta_\alpha + i\infty} \alpha(\zeta) A(\zeta) \exp(-p(\alpha y - \zeta x))\, d\zeta \right.$$
$$\left. - k_e^2 \int_{\zeta_\beta - i\infty}^{\zeta_\beta + i\infty} \beta(\zeta) A(\zeta) \exp(-p(\beta y - \zeta x))\, d\zeta \right), \tag{55}$$

$$D_x^*(x,y,p) = -\frac{e_{15}}{2\pi i} \int_{\zeta_\beta - i\infty}^{\zeta_\beta + i\infty} \zeta A(\zeta) \exp(-p(\beta y - \zeta x))\, d\zeta, \tag{56}$$

$$D_y^*(x,y,p) = \frac{e_{15}}{2\pi i} \int_{\zeta_\beta - i\infty}^{\zeta_\beta + i\infty} \beta(\zeta) A(\zeta) \exp(-p(\beta y - \zeta x))\, d\zeta, \tag{57}$$

where the integration paths are restricted by

$$-1/(c-v) < \zeta_\alpha < 1/(c+v), \tag{58}$$

$$-\varepsilon < \zeta_\beta < \varepsilon. \tag{59}$$

For displacement and electrostatic potential, the integral representations reduce to

$$w^*(x,y,p) = \frac{1}{2\pi i p} \int_{\zeta_\alpha - i\infty}^{\zeta_\alpha + i\infty} A(\zeta) \exp(-p(\alpha y - \zeta x))\, d\zeta, \tag{60}$$

$$\phi^*(x,y,p) = \frac{1}{2\pi i p}\frac{e_{15}}{\varepsilon_{11}}\left(\int_{\zeta_\alpha - i\infty}^{\zeta_\alpha + i\infty} A(\zeta)\exp(-p(\alpha y - \zeta x))\,d\zeta - \int_{\zeta_\beta - i\infty}^{\zeta_\beta + i\infty} A(\zeta)\exp(-p(\beta y - \zeta x))\,d\zeta\right). \tag{61}$$

3.2. *Wiener–Hopf*

In order to apply the Wiener–Hopf technique, it is expedient to expand the mechanical boundary conditions over the full range of the x-axis. This can be done by introducing new unknown functions in the usual way

$$\sigma_{yz}(x,0^+,t) = \sigma_+(x,t) - \delta(x+vt)H(t), \quad -\infty < x < \infty, \tag{62}$$

$$w(x,0^+,t) = w_-(x,t) + 0, \quad -\infty < x < \infty. \tag{63}$$

with

$$\sigma_+(x,t) \triangleq \begin{cases} \sigma_{xz}(x,0^+,t) & x \geqslant 0 \\ 0 & x < 0, \end{cases} \tag{64}$$

$$w_-(x,t) \triangleq \begin{cases} 0 & x \geqslant 0 \\ w(x,0^+,t) & x < 0. \end{cases} \tag{65}$$

After suppressing both x and t,

$$\hat{\sigma}^*_{yz}(\zeta,0^+,p) = -\frac{\bar{c}_{44}}{p}(\alpha(\zeta) - k_e^2\beta(\zeta))A(\zeta), \tag{66}$$

$$\hat{w}^*(\zeta,0^+,p) = \frac{A(\zeta)}{p^2}. \tag{67}$$

On the other hand, the transformed mechanical boundary conditions yield

$$\hat{\sigma}^*_{yz}(\zeta,0^+,p) = \frac{\Sigma_+(\zeta)}{p} + \frac{1}{pv}\frac{1}{(\zeta - 1/v)}, \tag{68}$$

$$\hat{w}^*(\zeta,0^+,p) = \frac{U_-(\zeta)}{p^2}, \tag{69}$$

where

$$\Sigma_+(\zeta) \triangleq p\int_0^\infty \sigma^*_+(x,p)\exp(-p\zeta x)\,dx, \tag{70}$$

$$U_-(\zeta) \triangleq p^2\int_{-\infty}^0 w^*_-(x,p)\exp(-p\zeta x)\,dx. \tag{71}$$

Comparison of (66) and (67), with (68) and (69) leads to

$$-\bar{c}_{44}(\alpha(\zeta)-k_e^2\beta(\zeta))A(\zeta) = \Sigma_+(\zeta)+\frac{1}{v}\frac{1}{(\zeta-1/v)}, \tag{72}$$

$$A(\zeta) = U_-(\zeta), \tag{73}$$

which leads to the standard Wiener–Hopf equation

$$\Sigma_+(\zeta)+\frac{1}{v(\zeta-1/v)} = K(\zeta)U_-(\zeta), \tag{74}$$

where

$$K(\zeta) \triangleq -\bar{c}_{44}(\alpha(\zeta)-k_e^2\beta(\zeta)). \tag{75}$$

The bracketed term is recognizable as the Bleustein–Gulyaev wave function. $K(\zeta)$ may be rewritten in the form

$$K(\zeta) = -\bar{c}_{44}(s-k_e^2)\sqrt{(1/(c_{bg}+v)-\zeta)(1/(c_{bg}-v)+\zeta)}S(\zeta), \tag{76}$$

where

$$S(\zeta) \triangleq \frac{(\alpha(\zeta)-k_e^2\beta(\zeta))}{(s-k_e^2)\sqrt{(1/(c_{bg}+v)-\zeta)(1/(c_{bg}-v)+\zeta)}}, \tag{77}$$

and

$$c_{bg} \triangleq \left(\frac{\bar{c}_{44}}{\rho}\right)^{1/2}\sqrt{1-k_e^4} \tag{78}$$

denotes the Bleustein–Gulyaev wave speed in a piezoelectric half space shielded with electrode (Bleustein, 1968; Gulyaev, 1969). Note that $S(\zeta) \to 1$, as $|\zeta| \to \infty$.

The key to solving the Wiener–Hopf equation (74) is the product factorization of $S(\zeta)$; that is, we seek factors such that

$$S(\zeta) = S_+(\zeta)S_-(\zeta), \tag{79}$$

where the functions $S_+(\zeta)$ and $S_-(\zeta)$ are sectionally analytic with respect to their respective half planes $P_+(\zeta)$ and $P_-(\zeta)$, where (see Fig. 2)

$$P_+(\zeta) \triangleq \{\zeta \in \mathbf{C} \mid \mathrm{Re}(\zeta) > -\varepsilon\}, \tag{80}$$

$$P_-(\zeta) \triangleq \{\zeta \in \mathbf{C} \mid \mathrm{Re}(\zeta) < \varepsilon\}. \tag{81}$$

Because of the simple structure of the Bleustein–Gulyaev wave function, one can find its roots exactly in simple algebraic form, which facilitates the ensuing product decomposition. From Fig. 2, it is evident that there are three branch points along each integration contour

$$\text{in } P_+(\zeta): \{-\varepsilon, -1/(c-v), -1/(c_{bg}-v)\},$$
$$\text{in } P_-(\zeta): \{-\varepsilon, -1/(c-v), -1/(c_{bg}-v)\}.$$

Consequently, the product decomposition here differs from that of the Rayleigh wave function, which only has two branch points along each integration contour

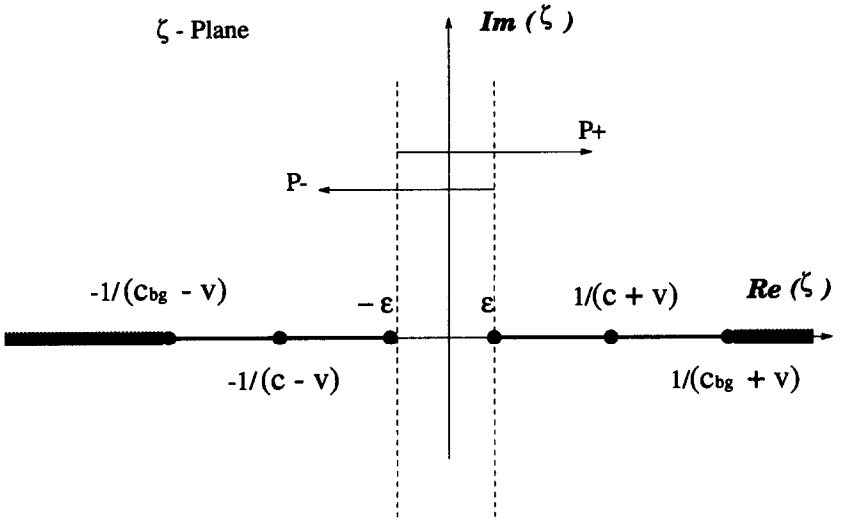

Fig. 2. Complex ζ-plane showing the locations of branch points of function $S(\zeta)$.

(Baker, 1962; Freund, 1990). The decomposition may be carried out by employing the Cauchy integral theorem to express the product terms as contour integrals around certain isolated branch cuts. The beauty of this approach is that one can form a precise factorization by evaluation of a contour integral, which is difficult to obtain by inspection. The details of this procedure may be found in Appendix A. The final product factorization results are listed here

$$\begin{cases} S_+(\zeta) = \sqrt{\dfrac{(1/(c_{bg}-v)+\zeta)}{(1/(c-v)+\zeta)}}\,\mathscr{S}_+(\zeta), \\ S_-(\zeta) = \sqrt{\dfrac{(1/(c_{bg}+v)-\zeta)}{(1/(c+v)-\zeta)}}\,\mathscr{S}_-(\zeta), \end{cases} \tag{82}$$

where

$$\begin{cases} \mathscr{S}_+(\zeta) \triangleq \exp\left\{-\dfrac{1}{\pi}\displaystyle\int_\varepsilon^{1/(c-v)} \arctan(\Xi(-\eta))\,\frac{d\eta}{\eta+\zeta}\right\}, \\ \mathscr{S}_-(\zeta) \triangleq \exp\left\{-\dfrac{1}{\pi}\displaystyle\int_\varepsilon^{1/(c+v)} \arctan(\Xi(\eta))\,\frac{d\eta}{\eta-\zeta}\right\}, \end{cases} \tag{83}$$

and

$$\Xi(\eta) \triangleq \frac{k_e^2\eta}{s(1/(c-v)+\eta)^{1/2}(1/(c+v)-\eta)^{1/2}}. \tag{84}$$

Functions $S_-(\zeta)$ and $S_+(\zeta)$ are analytic, single-valued and nonzero in the half plane $P_-(\zeta)$ and $P_+(\zeta)$, respectively. The overlap region is

$$-\varepsilon < \mathrm{Re}(\zeta) < \varepsilon, \tag{85}$$

as shown in Fig. 2.

Substituting (82) into (79) and (76), one can rearrange (74) such that

$$\frac{\Sigma_+(\zeta)D_+(\zeta)}{\sqrt{1/(c_{bg}-v)+\zeta}} + \frac{D_+(\zeta)}{v(\zeta-1/v)\sqrt{1/(c_{bg}-v)+\zeta}} = -\bar{c}_{44}(s-k_e^2)\sqrt{1/(c_{bg}-v)-\zeta}\,S_-(\zeta)U_-(\zeta), \tag{86}$$

where

$$D_+(\zeta) \triangleq \frac{1}{S_+(\zeta)}. \tag{87}$$

Let

$$F_+(\zeta) \triangleq \frac{D_+(\zeta)}{\sqrt{1/(c_{bg}-v)+\zeta}} = \frac{\sqrt{1/(c-v)+\zeta}}{(1/(c_{bg}-v)+\zeta)}\mathscr{D}_+(\zeta), \tag{88}$$

where

$$\mathscr{D}_+(1/v) \triangleq \frac{1}{\mathscr{S}_+(1/v)}. \tag{89}$$

Equation (86) can now be expressed as

$$\Sigma_+(\zeta)F_+(\zeta) + \frac{F_+(\zeta)}{v(\zeta-1/v)} = -\bar{c}_{44}(s-k_e^2)\frac{(1/(c_{bg}+v)-\zeta)}{\sqrt{1/(c_{bg}+v)-\zeta}}\mathscr{S}_-(\zeta)U_-(\zeta). \tag{90}$$

In order to separate the second term in (90) into two sectionally analytic functions, additive factorization is performed. By inspection, a possible additive decomposition is

$$\left(\frac{1}{v}\frac{1}{(\zeta-1/v)}(F_+(\zeta)-F_+(1/v))\right)_+ + \left(\frac{F_+(1/v)}{v(\zeta-1/v)}\right)_-, \tag{91}$$

where the constant $F_+(1/v)$ is evaluated as

$$F_+(1/v) = \sqrt{\frac{v}{c}}\frac{(c_{bg}-v)}{\sqrt{c-v}}\frac{\mathscr{D}_+(1/v)}{(1-k_e^4)^{1/2}}. \tag{92}$$

The Wiener–Hopf equation can be rearranged into the desired form

$$\Sigma_+(\zeta)F_+(\zeta) + \frac{1}{v(\zeta-1/v)}(F_+(\zeta)-F_+(1/v)) = -\bar{c}_{44}(s-k_e^2)\frac{(1/(c_{bg}+v)-\zeta)}{\sqrt{1/(c+v)-\zeta}}\mathscr{S}_-(\zeta)U_-(\zeta) - \frac{F_+(1/v)}{v(\zeta-1/v)}. \tag{93}$$

Equating both left and right hand side of (93) to an entire function, say $ET(\zeta)$,

$$ET(\zeta) = \Sigma_+(\zeta)F_+(\zeta) + \frac{1}{v(\zeta - 1/v)}(F_+(\zeta) - F_+(1/v)), \tag{94}$$

$$-ET(\zeta) = \bar{c}_{44}(s - k_e^2)\frac{(1/(c_{bg}+v)-\zeta)}{\sqrt{1/(c+v)-\zeta}}\mathscr{S}_-(\zeta)U_-(\zeta) + \frac{F_+(1/v)}{v(\zeta - 1/v)}. \tag{95}$$

Integrable energy density requires that as $x \to 0^+$,

$$|\sigma_+^*(x,p)| \sim \mathcal{O}(|x^{-1/2}|). \tag{96}$$

Continuity of displacement requires that as $x \to 0^-$, for some $q > 0$ it is the case that

$$|w_-^*(x,p)| \sim \mathcal{O}(|x^q|). \tag{97}$$

From the Abel theorem (van der Pol and Bremer, 1955), it follows that

$$\lim_{x \to 0^+} x^{1/2}\sigma_+^*(x,p) \sim \lim_{\zeta \to \infty} \zeta^{1/2}\Sigma_+(\zeta) \Rightarrow \Sigma_+(\zeta) \sim \mathcal{O}(\zeta^{-1/2}), \tag{98}$$

$$\lim_{x \to 0^-} |x|^{-q} w_-^*(x,p) \sim \lim_{|\zeta| \to \infty} |\zeta|^{1+q} U_-(\zeta) \Rightarrow U_-(\zeta) \sim \mathcal{O}(\zeta^{-((1/2)+q)}). \tag{99}$$

It follows that as $|\zeta| \to \infty$,

$$\left| \Sigma_+(\zeta)F_+(\zeta) + \frac{1}{v(\zeta - 1/v)}(F_+(\zeta) - F_+(1/v)) \right| \sim \mathcal{O}(|\zeta^{-1}|) \tag{100}$$

and

$$\left| \bar{c}_{44}(s - k_e^2)\frac{(1/(c_{bg}+v)-\zeta)}{\sqrt{1/(c_{bg}+v)-\zeta}}\mathscr{S}_-(\zeta)U_-(\zeta) + \frac{F_+(1/v)}{v(\zeta - 1/v)} \right| \sim \mathcal{O}(|\zeta^{-((1/2)+q)}|). \tag{101}$$

By the extended Liouville's theorem (Noble, 1958), the entire function $ET(\zeta)$ must be a polynomial of degree no greater than $\max(\lceil -(\frac{1}{2}+q) \rceil, \lceil -1 \rceil)$, that is, it must be identically zero. Hence,

$$U_-(\zeta) = -\frac{F_+(1/v)}{\bar{c}_{44}(s - k_e^2)}\frac{\sqrt{1/(c+v)-\zeta}}{(1/(c_{bg}+1)-\zeta)}\frac{\mathscr{D}_-(\zeta)}{v(\zeta - 1/v)}, \tag{102}$$

$$\Sigma_+(\zeta) = -\frac{1}{v(\zeta - 1/v)}\left[\frac{F_+(1/v)}{F_+(\zeta)} - 1\right], \tag{103}$$

where

$$\mathscr{D}_-(\zeta) \triangleq \frac{1}{\mathscr{S}_-(\zeta)} \tag{104}$$

or, in expanded form

$$U_-(\zeta) = -\frac{1}{\bar{c}_{44}}\frac{1}{\sqrt{v}}\frac{(s+k_e^2)}{(1-k_e^2)}\frac{1}{\sqrt{1-v/c}}\frac{\mathscr{D}_+(1/v)}{(1+v/c_{bg})}\frac{\sqrt{1/(c+v)-\zeta}}{1/(c_{bg}+v)-\zeta)}\frac{\mathscr{D}_-(\zeta)}{(\zeta - 1/v)} \tag{105}$$

and

$$\Sigma_+(\zeta) = \frac{1}{v}\frac{1}{(\zeta - 1/v)}\left[\frac{\sqrt{v}(1-v/c_{bg})}{\sqrt{1-v/c}}\frac{(1/(c_{bg}-v)+\zeta))}{\sqrt{1/(c-v)+\zeta}}\mathscr{S}_+(\zeta) - 1\right]. \tag{106}$$

4. FUNDAMENTAL SOLUTION IN PHYSICAL DOMAIN

Having carried out the Wiener–Hopf procedure, we are now in a position to invert the expressions (54)–(57), and (60)–(61), to obtain explicit solutions in the original physical domain. The exact inversion can be achieved by the Cagniard–de Hoop scheme (Cagniard, 1939; de Hoop, 1960).

4.1. *Inversion by Cagniard–de Hoop method*

We proceed by replacing the original Bromwich path by a deformed Cagniard contour such that the one-sided Laplace transform can be obtained by inspection. We seek contours in the ζ-plane (see Fig. 3) along which the exponentials in each integral of (54)–(61) take the form $\exp(-pt)$. To achieve this, we let

$$\alpha(\zeta)y - \zeta x = t. \tag{107}$$

Then the first set of deformed paths are obtained as

$$\zeta_{1\pm} = \frac{1}{x^2+s^2y^2}\left(-\left(tx+\frac{v}{c^2}y^2\right) \pm \mathrm{i}y\sqrt{s^2t^2 - \frac{2v}{c^2}xt - \frac{1}{c^2}(y^2+x^2)}\right). \tag{108}$$

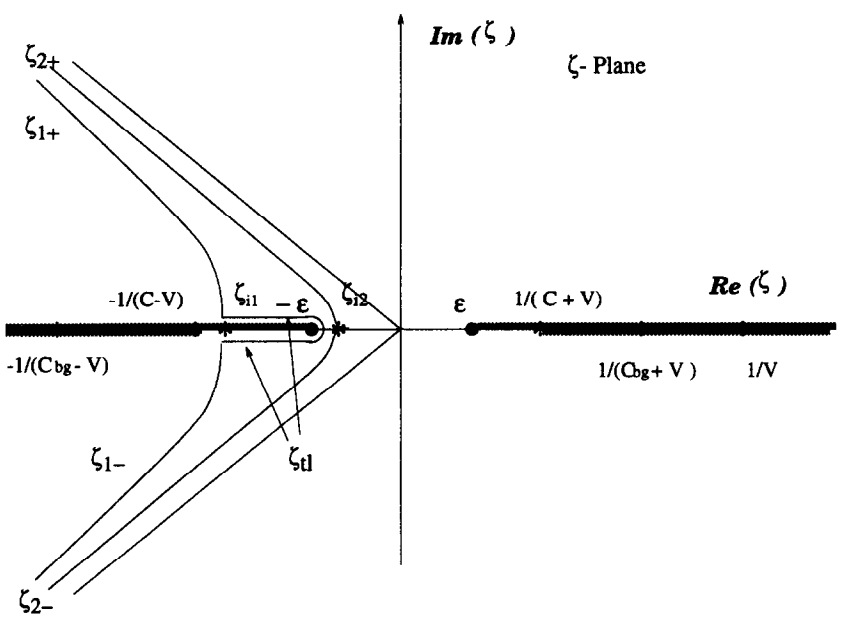

Fig. 3. Cagniard–de Hoop contours in ζ-plane.

Similarly, letting

$$\beta(\zeta)y-\zeta x = t \tag{109}$$

yields the second set of deformed paths

$$\zeta_{2\pm} = \frac{1}{r^2}\left(-xt \pm \mathrm{i}yt\sqrt{1-\varepsilon^2\frac{r^2}{t^2}}\right)$$

$$= \left(\frac{t}{r}\right)\left(-\cos\theta \pm \mathrm{i}\sin\theta\sqrt{1-\varepsilon^2\left(\frac{r}{t}\right)^2}\right), \tag{110}$$

where $r^2 \equiv x^2+y^2$.

The inversion path $\zeta_{1\pm}$ intercepts the Re(ζ) axis at the location

$$\zeta_{1i} = -\frac{1}{s^2c}\left[\frac{v}{c}+\frac{x}{\sqrt{x^2+s^2y^2}}\right], \quad \text{at } t_1 = \frac{1}{s^2}\left[\frac{vx}{c^2}+\frac{1}{c}\sqrt{x^2+s^2y^2}\right]. \tag{111}$$

Similarly, the second path $\zeta_{2\pm}$ intercepts the axis as

$$\zeta = -\varepsilon\frac{x}{r} = -\varepsilon\cos\theta, \quad \text{at } t_2 = \varepsilon r. \tag{112}$$

It is easy to verify that

$$\frac{-1}{c-v} < \zeta_{1i} < \frac{1}{c+v}, \tag{113}$$

and

$$-\varepsilon < \zeta_{2i} < \varepsilon. \tag{114}$$

As shown in Fig. 3, the contour $\zeta_{1\pm}$ may intercept the Re(ζ), axis through the branch cut, whereas the contours $\zeta_{2\pm}$ always avoid the cut. Therefore, for $\zeta_{1\pm}$, a supplemental contour ζ_{tl} may be needed consisting of two straight segments and a circle of radius $\delta(\delta \to 0)$ centered at the end of the branch cut at $\zeta = -\varepsilon$. The two segments are represented by

$$\zeta_{tl\pm} = \frac{1}{x^2+s^2y^2}\left(-\left(xt+\frac{v}{c^2}y^2\right)+y\sqrt{\frac{2vxt}{c^2}+\frac{r^2}{c^2}-s^2t^2}\right)\pm\mathrm{i}\delta, \tag{115}$$

and the range of t to which these expressions apply is

$$t_0 \leqslant t \leqslant t_1, \tag{116}$$

where

$$t_0 = \frac{y}{c}. \tag{117}$$

As a result of the foregoing manipulations, the inversion integrals along the Cagniard contours may be expressed as follows

$$\sigma^*_{xz}(x,y,p) = \frac{\bar{c}_{44}}{\pi}\int_{t_1}^{\infty} \mathrm{Im}\left[\zeta_{1+}U_-(\zeta_{1+})\frac{\partial\zeta_{1+}}{\partial t}\right]\exp(-pt)\,\mathrm{d}t$$
$$+\frac{1}{2}\int_{t_0}^{t_1} \mathrm{Im}\left[\zeta_{tl+}U_-(\zeta_{tl+})\frac{\partial\zeta_{tl+}}{\partial t} - \zeta_{tl-}U_-(\zeta_{tl-})\frac{\partial\zeta_{tl-}}{\partial t}\right]\exp(-pt)\,\mathrm{d}t$$
$$-k_e^2\int_{t_2}^{\infty} \mathrm{Im}\left[\zeta_{2+}U_-(\zeta_{2+})\frac{\partial\zeta_{2+}}{\partial t}\right]\exp(-pt)\,\mathrm{d}t\Bigg), \tag{118}$$

$$\sigma^*_{yz}(x,y,p) = -\frac{\bar{c}_{44}}{\pi}\Bigg(\int_{t_1}^{\infty} \mathrm{Im}\left[\alpha(\zeta_{1+})U_-(\zeta_{1+})\frac{\partial\zeta_{1+}}{\partial t}\right]\exp(-pt)\,\mathrm{d}t$$
$$+\frac{1}{2}\int_{t_0}^{t_1} \mathrm{Im}\left[\alpha(\zeta_{tl+})U_-(\zeta_{tl+})\frac{\partial\zeta_{tl+}}{\partial t} - \alpha(\zeta_{tl-})U_-(\zeta_{tl-})\frac{\partial\zeta_{tl-}}{\partial t}\right]\exp(-pt)\,\mathrm{d}t$$
$$-k_e^2\int_{t_2}^{\infty} \mathrm{Im}\left[\beta(\zeta_{2+})U_-(\zeta_{2+})\frac{\partial\zeta_{2+}}{\partial t}\right]\exp(-pt)\,\mathrm{d}t\Bigg), \tag{119}$$

$$D^*_x(x,y,p) = -\frac{e_{15}}{\pi}\Bigg(\int_{t_2}^{\infty} \mathrm{Im}\left[\zeta_{2+}U_-(\zeta_{2+})\frac{\partial\zeta_{2+}}{\partial t}\right]\exp(-pt)\,\mathrm{d}t\Bigg), \tag{120}$$

$$D^*_y(x,y,p) = \frac{e_{15}}{\pi}\Bigg(\int_{t_2}^{\infty} \mathrm{Im}\left[\beta(\zeta_{2+})U_-(\zeta_{2+})\frac{\partial\zeta_{2+}}{\partial t}\right]\exp(-pt)\,\mathrm{d}t\Bigg), \tag{121}$$

and

$$w^*(x,y,p) = \frac{1}{\pi p}\Bigg(\int_{t_1}^{\infty} \mathrm{Im}\left[U_-(\zeta_{1+})\frac{\partial\zeta_{1+}}{\partial t}\right]\exp(-pt)\,\mathrm{d}t$$
$$+\frac{1}{2}\int_{t_0}^{t_1} \mathrm{Im}\left[U_-(\zeta_{tl+})\frac{\partial\zeta_{tl+}}{\partial t} - U_-(\zeta_{tl-})\frac{\partial\zeta_{tl-}}{\partial t}\right]\exp(-pt)\,\mathrm{d}t\Bigg), \tag{122}$$

$$\phi^*(x,y,p) = \frac{1}{\pi p}\frac{e_{15}}{\varepsilon_{11}}\Bigg(\int_{t_1}^{\infty} \mathrm{Im}\left[U_-(\zeta_{1+})\frac{\partial\zeta_{1+}}{\partial t}\right]\exp(-pt)\,\mathrm{d}t$$
$$+\frac{1}{2}\int_{t_0}^{t_1} \mathrm{Im}\left[U_-(\zeta_{tl+})\frac{\partial\zeta_{tl+}}{\partial t} - U_-(\zeta_{tl-})\frac{\partial\zeta_{tl-}}{\partial t}\right]\exp(-pt)\,\mathrm{d}t$$
$$-\int_{t_2}^{\infty} \mathrm{Im}\left[U_-(\zeta_{2+})\frac{\partial\zeta_{2+}}{\partial t}\right]\exp(-pt)\,\mathrm{d}t\Bigg). \tag{123}$$

Since $\alpha(\zeta)$, ζ, and $U_-(\zeta)$ are all analytic along the strip $-1/(c-v) < \mathrm{Re}(\zeta) < -\varepsilon$, all of the integrals along the supplemental path ζ_{tl} vanish. Thus, closed form solutions are available as follows

$$\sigma_{xz}(x,y,t) = \frac{\bar{c}_{44}}{\pi}\left(H(t-t_1)\,\mathrm{Im}\left[\zeta_{1+}U_-(\zeta_{1+})\frac{\partial\zeta_{1+}}{\partial t}\right] - k_e^2 H(t-t_2)\mathrm{Im}\left[\zeta_{2+}U_-(\zeta_{2+})\frac{\partial\zeta_{2+}}{\partial t}\right]\right), \tag{124}$$

$$\sigma_{yz}(x,y,t) = -\frac{\bar{c}_{44}}{\pi}\left(H(t-t_1)\,\mathrm{Im}\left[\alpha(\zeta_{1+})U_-(\zeta_{1+})\frac{\partial\zeta_{1+}}{\partial t}\right] - k_e^2 H(t-t_2)\mathrm{Im}\left[\beta(\zeta_{2+})U_-(\zeta_{2+})\frac{\partial\zeta_{2+}}{\partial t}\right]\right), \tag{125}$$

$$D_x(x,y,t) = \frac{e_{15}}{\pi}H(t-t_2)\,\mathrm{Im}\left[\zeta_{2+}U_-(\zeta_{2+})\frac{\partial\zeta_{2+}}{\partial t}\right], \tag{126}$$

$$D_y(x,y,t) = -\frac{e_{15}}{\pi}H(t-t_2)\,\mathrm{Im}\left[\beta(\zeta_{2+})U_-(\zeta_{2+})\frac{\partial\zeta_{2+}}{\partial t}\right], \tag{127}$$

and

$$w(x,y,t) = \frac{1}{\pi}\int_{t_1}^{t}\mathrm{Im}\left[U_-(\zeta_{1+}(\tau))\frac{\partial\zeta_{1+}(\tau)}{\partial\tau}\right]\mathrm{d}\tau, \tag{128}$$

$$\phi(x,y,t) = \frac{1}{\pi}\frac{e_{15}}{\varepsilon_{11}}\left(\int_{t_1}^{t}\mathrm{Im}\left[U_-(\zeta_{1+}(\tau))\frac{\partial\zeta_{1+}(\tau)}{\partial\tau}\right]\mathrm{d}\tau - \int_{t_2}^{t}\mathrm{Im}\left[U_-(\zeta_{2+}(\tau))\frac{\partial\zeta_{2+}(\tau)}{\partial\tau}\right]\mathrm{d}\tau\right). \tag{129}$$

It may be verified that as the electro-mechanical coupling coefficient $k_e \to 0$, the above solutions recover the solution for anti-plane crack propagation in a purely elastic medium (Ma and Chen, 1992).

4.2. *Asymptotic solution*

For purposes of fracture analysis, most of the significance of these results is encapsulated in the near-tip fields of the running crack. When $y = 0$, both inversion contours take the same path $\zeta_{1+} = \zeta_{2+} = \zeta_+$, i.e.

$$\begin{cases} \zeta_+ = -\dfrac{t}{x}, \\ \dfrac{\partial\zeta_+}{\partial t} = -\dfrac{1}{x}. \end{cases} \tag{130}$$

It follows that ahead of the moving crack tip, $x \to 0^+ (\varepsilon \to 0)$,

$$\sigma_{yz}(x,0^+,t)=\frac{1}{\pi}\frac{(s+k_e^2)}{\sqrt{vc}}\frac{c^2}{(1-k_e^4)^{1/2}}\frac{\mathscr{D}_+(1/v)}{\sqrt{c-v}}\frac{\sqrt{t+x/(c+v)}}{(c_{bg}+v)}$$
$$\cdot\frac{(s\sqrt{(t-x/(c-v))(t+x/(c+v))}-k_v^2 t)}{(t+x/v)(t+x/(c_{bg}+v))}\frac{\mathscr{D}_-(-t/x)}{\sqrt{x}},\quad t>t_1, \tag{131}$$

$$D_y(x,0^+,t)=\frac{1}{\pi}\frac{e_{15}}{\bar{c}_{44}}\frac{(s+k_e^2)}{\sqrt{vc}}\frac{c^2}{(1-k_e^4)^{1/2}}\frac{1}{\sqrt{c-v}}\frac{\mathscr{D}_+(1/v)}{(c_{bg}+v)}$$
$$\cdot\frac{t\sqrt{t+x/(c+v)}}{(t+x/v)(t+x/(c_{bg}+v))}\frac{D_-(-t/x)}{\sqrt{x}},\quad t>t_2. \tag{132}$$

As $x\to 0^+$, $t/x\to\infty$,

$$\mathscr{D}_-(-t/x)\to 1 \tag{133}$$

and the asymptotic stress field ahead of crack tip reduces to

$$\sigma_{yz}(x,0^+,t)\sim\frac{1}{\pi}\frac{(1-v/c_{bg})}{\sqrt{1-v/c}}\frac{\mathscr{D}_+(1/v)}{\sqrt{v}}\frac{1}{\sqrt{xt}}+\mathscr{O}(1) \tag{134}$$

and the asymptotic electric displacement field to

$$D_y(x,0^+,t)\sim\frac{1}{\pi}\frac{e_{15}}{\bar{c}_{44}}\frac{(s+k_e^2)}{\sqrt{vc}}\frac{c^2}{(1-k_e^4)^{1/2}}\frac{1}{\sqrt{c-v}}\frac{\mathscr{D}_+(1/v)}{(c_{bg}+v)}\frac{1}{\sqrt{xt}}+\mathscr{O}(1). \tag{135}$$

It can be seen from (134) and (135) that both stress and electric displacement exhibit a square root singularity as the crack tip is approached.

4.3. *Intensity factors*

Before expressing the usual dynamic intensity factors, the result above may be generalized in a familiar way (Freund, 1972a) to the distributed loading case. For example, assume a general antisymmetric external load distribution, $p(X)$, over the newly formed crack surface ($0<X<vt$). The general stress field and electric displacement field ahead of the crack tip are then obtained from the fundamental solutions as

$$\sigma^{(g)}(x,t)=\int_0^{vt}\sigma_{yz}\left(x,0,t-\frac{X}{v}\right)p(X)\,dX, \tag{136}$$

$$D_y^{(g)}(x,t)=\int_0^{vt}D_y\left(x,0,t-\frac{X}{v}\right)p(X)\,dX, \tag{137}$$

where the superscript (g) indicates that the field is induced by the general traction load distribution.

Making the change of variable $vt-X=\eta$ and introducing

$$P(l) \triangleq \sqrt{\frac{2}{\pi}} \int_0^l \eta^{-1/2} p(l-\eta)\, d\eta, \tag{138}$$

the dynamic stress intensity factor for this general load distribution is

$$K_{IIIT}^{(\sigma)}(vt, v) \triangleq \lim_{x\to 0} \sqrt{2\pi x}\sigma^{(g)}(x, t)$$

$$= \frac{(1-v/c_{bg})}{\sqrt{1-v/c}} \mathscr{D}_+(1/v) P(vt), \tag{139}$$

and the electric displacement intensity factor is

$$K_{IIIT}^{(D)}(vt, v) \triangleq \lim_{x\to 0} \sqrt{2\pi x} D_y^{(g)}(x, t)$$

$$= \frac{\varepsilon_{11}}{e_{15}} \frac{k_e^2}{(1-k_e^4)} \frac{(s+k_e^2)}{(1+v/c_{bg})} \frac{\mathscr{D}_+(1/v)}{\sqrt{1-c/v}} P(vt), \tag{140}$$

where the following decoration of the intensity factors is adopted: the superscript [(σ) or (D)] indicates stress or electric displacements; the subscript $(IIIT)$ indicates that the loading is an antiplane traction loading.

For crack problems in piezoelectric materials, even in the static case (Pak, 1992b; Zhang and Hack, 1992), careful distinction between intensity factors must be maintained, because of the possibilities for different combinations of loading and boundary conditions (mechanical and electrical). The various cases for dynamic crack propagation will be dealt with systematically in Part II of this work.

Following Freund (1972a), it is convenient to introduce a normalization based on the corresponding "quasi-static" intensity factors. The relevant intensity factors are

$$K_{IIIT}^{(\sigma)}(vt, 0) = P(vt) \tag{141}$$

and

$$K_{IIIT}^{(D)}(vt, 0) = \frac{\varepsilon_{11}}{e_{15}} \frac{k_e^2}{1-k_e^2} P(vt). \tag{142}$$

Hence, the dynamic intensity factors can be expressed as

$$K_{IIIT}^{(\sigma)}(vt, v) = f(v) K_{IIIT}^{(\sigma)}(vt, 0), \tag{143}$$

$$K_{IIIT}^{(D)}(vt, v) = g(v) K_{IIIT}^{(D)}(vt, 0), \tag{144}$$

where

$$f(v) \triangleq \frac{(1-v/c_{bg})}{\sqrt{1-v/c}} \mathscr{D}_+(1/v) \tag{145}$$

and

$$g(v) \triangleq \frac{(s+k_e^2)}{(1+k_e^2)} \frac{1}{(1+v/c_{bg})} \frac{\mathscr{D}_+(1/v)}{\sqrt{1-v/c}} \tag{146}$$

are the nondimensional dynamic intensity factors.

As is the case for the normalized stress intensity factor in the elastodynamic case [to which $f(v)$ reduces when $k_e \to 0$], both functions $f(v)$ and $g(v)$ are independent of the load distribution function $p(X)$ and the crack extension distance vt. They only depend on crack speed and the material constants, which include the shear wave speed c, the Bleustein–Gulyaev wave speed c_{bg} and the electro-mechanical coupling factor k_e. That is, f and g are universal functions of piezoelectric dynamic crack growth.

5. DISCUSSION

Before examining the detailed characteristics of the universal functions f and g, the physical context may be set by tabulating properties for several commonly used piezoelectric materials (Table 1). (It should be noted that even for the same material these properties may vary with factors such as manufacturer and year of production.) The corresponding piezoelectrically stiffened Young's modulus, bulk shear wave speed, electro-mechanical coupling coefficient, and the Bleustein–Gulyaev wave speed are shown in Table 2. The materials chosen in the illustration cover a fairly large range of electro-mechanical coupling coefficient; usually the Bleustein–Gulyaev wave speed is quite close to the bulk shear wave speed.

For these parameter values, the universal functions $f(v)$ and $g(v)$ have been plotted against crack propagation speed, normalized by Bleustein–Gulyaev wave speed. Figure 4 displays the results for two compounds PZT 65/35 and ZnO.

The behavior of the universal function $f(v)$ is similar to the universal function $k_{III}(v)$ of purely elastic solids, to which it of course reduces when $k_e = 0$. However, the behavior of the normalized dynamic electric displacement intensity factor, $g(v)$, is qualitatively different. It does not monotonically decrease as crack velocity increases, but after an initial decrease as the crack speed increases from zero, increases again as the Bleustein–Gulyaev speed is approached.

Table 1. *Material properties of several piezoelectric media*

Compound	ρ (density) (10^3 kg/m^3)	ε_{11}^S (10^{-9} F/m)	c_{44}^E (10^{10} N/m^2)	e_{15} (C/m)
PZT-4[a]	7.5	6.4634	2.56	12.7
PZT-5[a]	7.75	8.1103	2.11	12.3
$BaTiO_3$[a]	5.7	9.8722	4.4	11.4
PZT 65/35[b]	7.825	5.66	3.890	8.387
ZnO[c]	5.68	0.0757	4.247	−0.48

[a]Berlincourt *et al.*, 1964
[b]Chen, 1983
[c]Auld, 1973

Table 2. *Electroacoustic constants of several piezoelectric materials*

Compound	$\bar{c}_{44} \equiv c_{44}^E + \frac{e_{15}^2}{\varepsilon_{11}}$ (10^{10} N/m^2)	$k_e = \sqrt{\frac{e_{15}^2}{\bar{c}_{44} e_{11}^S}}$	$c \equiv \sqrt{\frac{\bar{c}_{44}}{\rho}}$ (10^3 m/s)	$c_{bg} \equiv c\sqrt{1-k_e^4}$ (10^3 m/s)
PZT-4[a]	5.0554	0.7026	2.5963	2.2579
PZT-5[a]	3.9754	0.6850	2.2649	2.000
$BaTiO_3$[a]	5.7164	0.4799	3.1668	3.0817
PZT 65/35[b]	5.1328	0.4921	3.9045	3.7883
ZnO[c]	4.5514	0.2586	3.5327	3.5248

[a]Berlincourt *et al.*, 1964
[b]Chen, 1983
[c]Auld, 1973

Examining this a little further, Fig. 5 displays $f(v)$ for a broader range of electromechanical coefficients ($k_e =$ 0.00, 0.30, 0.60, 0.90, 0.99), and plots against two different dimensionless velocities v/c and v/c_{bg}. For $k_e = 0.0$, the elastodynamic result is recovered

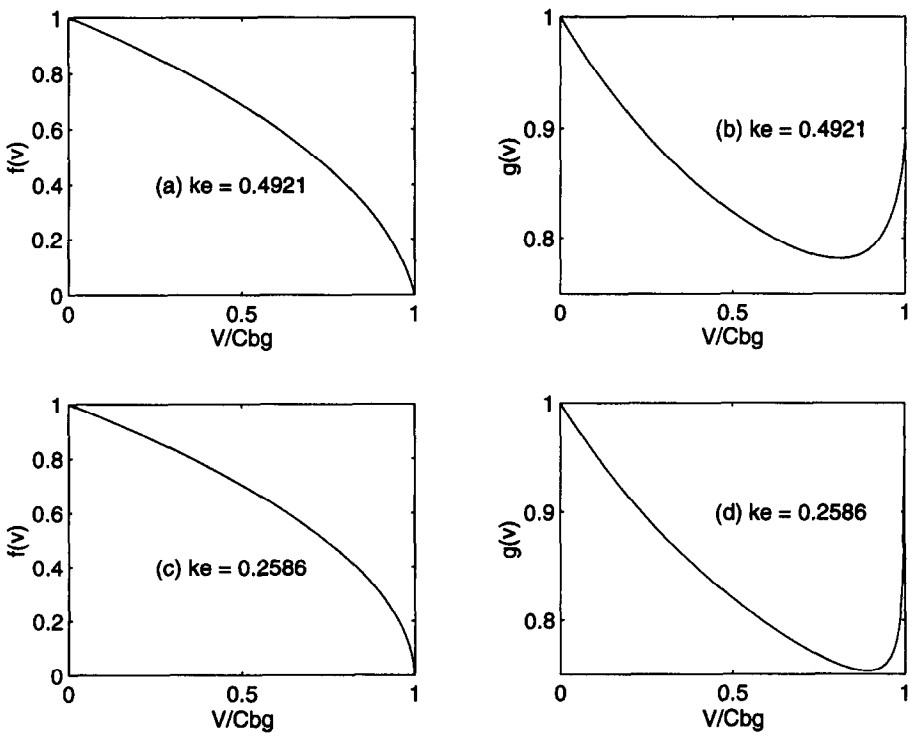

Fig. 4. Comparison between dynamic stress intensity factor $f(v)$ and dynamic electric displacement intensity factor ($g(v)$): (a) $f(v)$ for PZT65/35; (b) $g(v)$ for PZT65/35; (c) $f(v)$ for ZnO; (d) $g(v)$ for ZnO.

$$f(v) = k_{III}(v) = \sqrt{1-v/c}. \tag{147}$$

For larger values of k_e, the curve shape flattens [Fig. 5(b)], but the major contribution to suppression of stress intensity is the divergence of the Bleustein–Gulyaev wave speed from the bulk shear wave speed (though rather large values of k_e are required for this effect to be pronounced). This vanishing of stress intensity at the surface wave speed is analogous to the case of in-plane crack extension for purely elastic materials, for which the limiting speed is the Rayleigh wave speed rather than the bulk longitudinal wave speed. Curiously, it is in sharp contrast with the classical anti-plane crack propagation problem in purely elastic materials (Kostrov, 1966; Sih and Chen, 1977), for which the bulk shear wave speed is the critical speed.

The behavior of $g(v)$ is a little less straightforward (Fig. 6). As v approaches c_{bg}, $g(v)$ attains a finite nonzero value

$$g(c_{bg}) = \frac{k_e^2}{(1+k_e^2)} \frac{\mathscr{D}_+(1/c_{bg})}{\sqrt{1-\sqrt{1-k_e^4}}}. \tag{148}$$

However, there is some boundary layer character with respect to electro-mechanical coefficient k_e. That is, the following limit processes are not interchangeable

$$\lim_{k_e\to 0}\lim_{v\to c_{bg}} g(v,k_e) \neq \lim_{v\to c_{bg}}\lim_{k_e\to 0} g(v,k_e). \tag{149}$$

As a matter of fact, one can obtain $\mathscr{D}_+(1/v)$ explicitly

$$\mathscr{D}_+(1/v) = \sqrt{\frac{s(1+k_e^2)}{s+k_e^2}}, \tag{150}$$

so that

$$\lim_{k_e\to 0}\lim_{v\to c_{bg}} g(v) = 1. \tag{151}$$

On the other hand, at $k_e = 0.0$

$$g(v) = \frac{1}{\sqrt{1+v/c}}, \tag{152}$$

which leads to

$$\lim_{v\to c_{bg}}\lim_{k_e\to 0} g(v) = \frac{1}{\sqrt{2}}. \tag{153}$$

In general, the electrical contribution to the energy release rate must be taken into account, in which case the behavior of $g(v)$ would be significant for crack propagation. For the particular case of the "electrode" boundary condition considered here, the electrostatic potential is zero both along the line ahead of the crack and on the crack faces; consequently, for this case (but not for other choices of boundary condition or loading) there is no contribution from electric field to the energy release rate. The energy release rate can be calculated in a way analogous to the elastic case, for example (Atkinson and Eshelby, 1967).

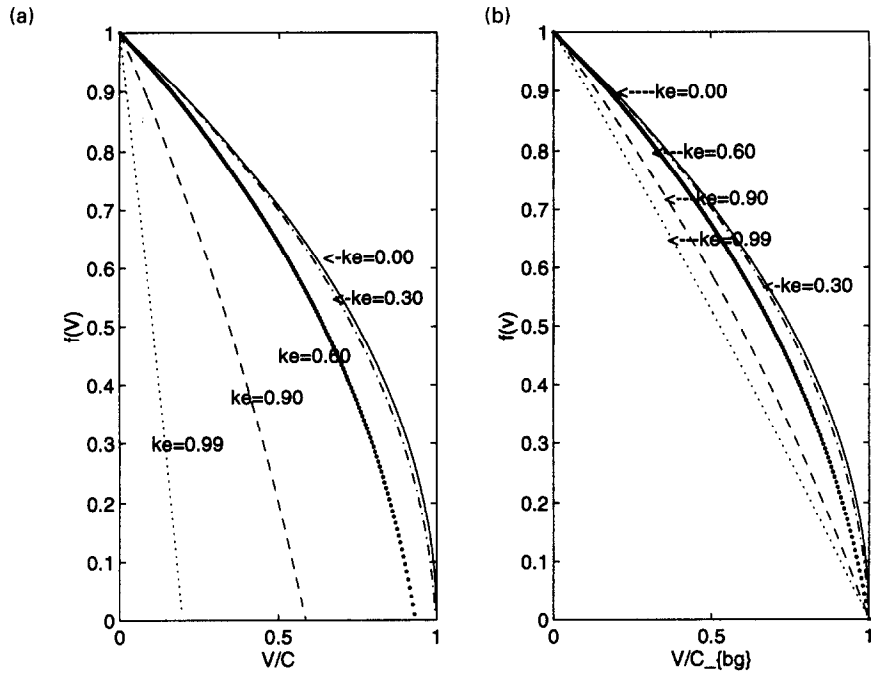

Fig. 5. Variations of universal function $f(v)$: (a) $f(v)$ versus v/c ; (b) $f(v)$ versus v/c_{bg}.

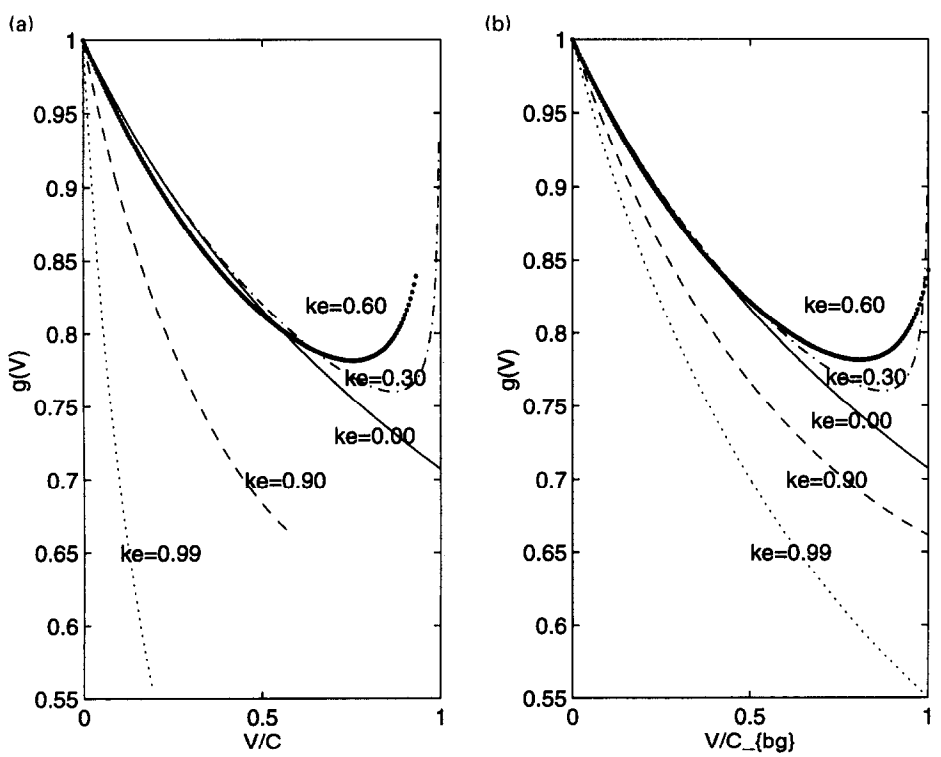

Fig. 6. Variations of universal function $g(v)$: (a) $g(v)$ versus v/c ; (b) $g(v)$ versus v/c_{bg}.

$$G(vt, v) \triangleq 2 \lim_{l \to 0} \int_{-l}^{l} \left[\sigma_{yz}(x, 0, t) \frac{\partial w}{\partial x}(x, 0, t) + D_y(x, 0, t) \frac{\partial \phi}{\partial x}(x, 0, t) + vE \right] dx$$

$$= 2 \lim_{l \to 0} \int_{-l}^{l} \sigma_{yz}(x, 0, t) \frac{\partial w}{\partial x}(x, 0, t)\, dx. \tag{154}$$

Making use of the identity (Freund, 1972b)

$$\lim_{\ell \to 0} \int_{-\ell}^{\ell} \frac{H(x)}{\sqrt{x}} \frac{H(-x)}{\sqrt{-x}} dx = \frac{\pi}{2} \tag{155}$$

yields

$$G(vt, v) = \frac{1}{2\bar{c}_{44}} \frac{c^2(s + k_e^2)}{(c_{bg} - v)(c_{bg} + v)} (K_{III}^{(\sigma)}(vt, v))^2. \tag{156}$$

A convenient normalization is to the quasi-static elastic result

$$G_{00}(vt) \triangleq \frac{1}{2c_{44}} (P(vt))^2. \tag{157}$$

The normalized energy release rate then reduces to

$$\frac{G(vt, v)}{G_{00}(vt)} = \sqrt{\frac{(1 + v/c)}{(1 - v/c)}} \frac{(1 - v/c_{bg})}{(1 + v/c_{bg})}. \tag{158}$$

As $k_e \to 0$, (158) reduces to the purely elastic results (e.g. Eshelby, 1969)

$$\frac{G(vt, v)}{G_{00}(vt)} = \sqrt{\frac{(1 - v/c_0)}{(1 + v/c_0)}}, \tag{159}$$

where

$$c_0 = \sqrt{\frac{c_{44}}{\rho}} \tag{160}$$

is the elastic shear wave speed.

It is of interest to look at the preceding results from the point of view of a material with fixed elastic properties as piezoelectric coupling increases. Figure 7 shows the profiles of the normalized energy release rate at different values of k_e, plotted against v/c_0. For $v = 0$ there is no effect of piezoelectricity on energy release rate; the result coincides with the elastic result for the same loading. There are two competing wave-speed effects: the bulk shear wave speed c increases with k_e for fixed c_0, and the ratio c_{bg}/c decreases with increasing k_e. However, since $c_{bg}/c_0 = \sqrt{1 + k_e^2}$, the former effect dominates, and the overall effect is to increase the energy release rate for a given crack speed and loading.

Nevertheless, the Bleustein–Gulyaev wave speed provides for this case the limiting velocity for crack propagation, just as the Rayleigh wave does for the in-plane elastic case. For this reason, we have not in this paper discussed the supersonic crack velocity

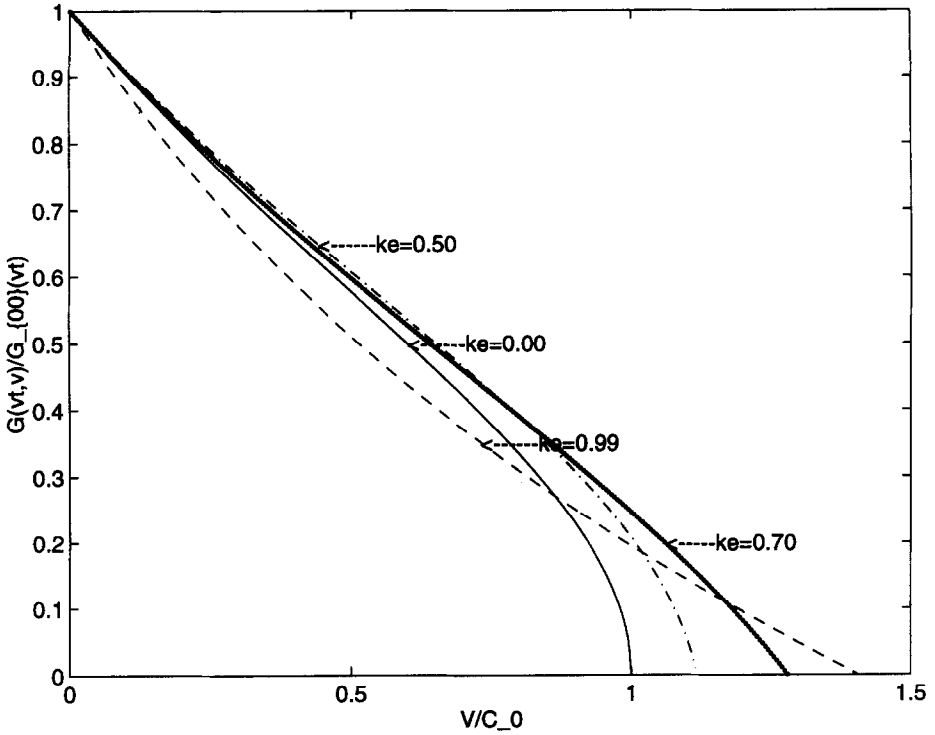

Fig. 7. The normalized energy release rate $G(vt, v)/G_{00}(vt)$ versus v/c_0.

regimes for which v exceeds c_{bg}. This discussion is deferred until the second part of this work, in which we describe the much richer behavior arising when vacuum boundary conditions are applied.

ACKNOWLEDGEMENTS

The work of the authors was partially supported by the Walter P. Murphy Fellowship from Northwestern University (SL), and by grant DMD-9057626 from the National Science Foundation (PAM). The comments, suggestions and literature references provided by the anonymous reviewers of an earlier draft of this paper are also gratefully acknowledged.

REFERENCES

Achenbach, J. D. (1973) *Wave Propagation in Elastic Solids*. North-Holland, Amsterdam.
Atkinson, C. and Eshelby, J. D. (1967) The flow of energy into the tip of a moving crack. *Int. J. Fracture* **4**, 3–8.
Auld, B. A. (1973) *Acoustic Fields and Waves in Solids*. John Wiley & Sons, New York.
Baker, B. R. (1962) Dynamic stress created by a moving crack. *J. Appl. Mech.* **29**, 449–458.
Bailey, T. and Hubbard, Jr, J. E. (1985) Distributed piezoelectric-polymer active vibration control of a cantilever beam. *J. Guidance Control* **8**, 605–611.
Berlincourt, D. A., Curran, D. R. and Jaffe, H. (1964) Piezoelectric and piezomagnetic materials

and their function in transducers. *Physical Acoustics* (ed. W. P. Mason), pp. 169–270. Academic Press, New York.

Bleustein, J. L. (1968) A new surface wave in piezoelectric materials. *Appl. Phys. Lett.* **13,** 412–413.

Broberg, K. B. (1973) On dynamic crack propagation in elastic–plastic media. *Proceedings of the International Conference on Dynamic Crack Propagation* (ed. G. C. Sih), pp. 461–499. Noordhoff International, Amsterdam.

Cady, W. G. (1946) *Piezoelectricity*. McGraw-Hill, New York.

Cagniard, L. (1939) *Reflexion et Refraction des Ondes Seismiques Progressives*. Gauthier-Villars, Paris. English translation *Reflection and Refraction of Progressive Seismic Waves*, E. A. Flinn and C. H. Dix, 1962, McGraw-Hill, New York.

Chen, P. J. (1983) Characterization of the three dimensional properties of poled PZT 65/35 in the absence of losses. *Acta Mech.* **47,** 95–106.

Deeg, W. F. (1980) The analysis of dislocation, crack and inclusion problems in piezoelectric solids. Ph.D. thesis, Stanford University.

de Hoop, A. T. (1960) A modification of Cagniard's method for solving seismic pulse problems. *Appl. Sci. Res. B* **8,** 349–360.

Duffy, D. G. (1994) *Transform Methods for Solving Partial Differential Equations*. CRC Press, Ann Arbor.

Eshelby, J. D. (1969) The starting of a crack. *Physics of Strength and Plasticity* (ed. A. S. Argon), pp. 263–275. MIT Press, Cambridge, MA.

Freund, L. B. (1972) Crack propagation in an elastic solid subjected to general loading. I: constant rate of extension. *J. Mech. Phys. Solids* **20,** 120–140.

Freund, L. B. (1972) Energy flux into the tip of an extending crack in an elastic solid. *J. Elasticity* **2,** 341–349.

Freund, L. B. (1990) *Dynamic Fracture Mechanics*. Cambridge University Press, Cambridge.

Gulyaev, Y. V. (1969) Electroacoustic surface waves in solids. *Soviet Physics JETP* **9,** 37–38.

Kostrov, B. V. (1966) Unsteady propagation of longitudinal shear cracks. *J. Appl. Math. Mech.* **30,** 1241–1248. Original paper in Russian is in *Prikladnaia Matematika I Mekhanika* **30,** 1042–1049.

Li, S., Cao, W. and Cross, L. E. (1990) Stress and electric displacement distribution near Griffith's type III crack tips in piezoceramics. *Mater. Lett.* **10,** 219–222.

Li, S. (1996) The electromagneto-acoustic surface wave in a piezoelectric medium: the Bleustein–Gulyaev mode, to appear in *J. Appl. Phys.*

Ma, C.-C. and Chen, S.-K. (1992) Investigation on the stress intensity factor field for unstable dynamic crack growth. *Int. J. Fracture* **58,** 345–359.

McMeeking, R. M. (1989) Electrostrictive stress near crack-like flaws. *Zeitschrift für Angewandte Mathematik und Physik* **40,** 615–627.

McMeeking, R. M. (1989) On mechanical stresses at cracks in dielectrics with application to dielectric breakdown. *J. Appl. Phys.* **62,** 3116–3122.

McMeeking, R. M. (1990) A J-integral for the analysis of electrically induced mechanical stress at cracks in elastic dielectrics. *Int. J. Engng Sci.* **28,** 605–613.

Maugin, G. A. (1983) Elastic surface waves with transverse horizontal polarization. *Advances in Applied Mechanics* (ed. C. S. Yih), Vol. 23, pp. 373–434. Academic Press, New York.

Maugin, G. A. (1993) *Material Inhomogenieties in Elasticity*. Chapman & Hall, London.

Maugin, G. A. (1994) On the J-integral and energy-release rate in dynamical fracture. *Acta Mech.* **105,** 33–47.

Noble, B. (1958) *Methods Based on the Wiener–Hopf Technique*. Pergamon Press, New York.

Pak, Y. E. (1990) Crack extension force in a piezoelectric material. *J. Appl. Mech.* **57,** 647–653.

Pak, Y. E. (1992) Circular inclusion problem in antiplane piezoelectricity. *Int. J. Solids Struct.* **29,** 2403–2419.

Pak, Y. E. (1992) Linear electro–elastic fracture mechanics of piezoelectric materials. *Int. J. Fracture* **54,** 79–100.

Parton, V. Z. (1976) Fracture mechanics of piezoelectric materials. *Acta Astronautica* **3,** 671–683.

Parton, V. Z. and Kudryatvsev, B. A. (1988) *Electromagnetoelasticity*. Gordon and Breach, New York.
Pohanka, R. C. and Smith, P. L. (1988) Recent advances in piezoelectric ceramics. *Electronic Ceramics* (ed. L. M. Levinson). Marcel Dekker, New York.
Rao, S. S. and Sunar, M. (1994) Piezoelectricity and its use in disturbance sensing and control of flexible structures: a survey. *Appl. Mech. Rev.* **47,** 113–123.
Sih, G. C. and Chen, E. P. (1977) Cracks moving at constant velocity and acceleration. *Mechanics of Fracture* 4: *Elastodynamic Crack Problems* (ed. G. C. Sih), pp. 59–117. Noordhoff, Amsterdam.
Sosa, H. A. (1990) Three-dimensional eigenfunction analysis of a crack in a piezoelectric material. *Int. J. Solids Struct.* **26,** 1–15.
Sosa, H. A. (1991) Plane problems in piezoelectric media with defects. *Int. J. Solids Struct.* **28,** 491–505.
Sosa, H. A. (1992) On the fracture mechanics of piezoelectric solids. *Int. J. Solids Struct.* **29,** 2613–2622.
Suo, Z., Kuo, C.-M., Barnett, D. M. and Willis, J. R. (1992) Fracture mechanics for piezoelectric ceramics. *J. Mech. Phys. Solids*, **40,** 739–765.
Suo, Z. (1993) Models for breakdown-resistant dielectric and ferroelectric ceramics. *J. Mech. Phys. Solids* **41,** 1155–1176.
Tiersten, H. F. (1969) *Linear Piezoelectric Plate Vibrations*. Plenum Press, New York.
van der Pol, B. and Bremer, H. (1955) *Operational Calculus*, 2nd edn. Cambridge University Press, Cambridge.
Viktorov, I. A. (1981) *Surface Sound Waves in Solids*. Nauka, Moscow (in Russian).
Wang, B. (1992) Three-dimensional analysis of a flat elliptical crack in a piezoelectric material. *Int. J. Engng Sci.* **30,** 781–791.
Zhang, T.-Y. and Hack, J. E. (1992) Mode-III crack in piezoelectric materials. *J. Appl. Phys.* **71,** 5865–5870.

APPENDIX A: PRODUCT DECOMPOSITION OF $S(\zeta)$

This appendix outlines the derivation of the product decomposition of an expression involving the Bleustein–Gulyaev function $\alpha(\zeta)-k_e^2\beta(\zeta)$. This factorization provides the essential ingredient in solving the Wiener–Hopf equation (86).

From (77), the expression of interest is

$$S(\zeta) \triangleq \frac{\alpha(\zeta)-k_e^2\beta(\zeta)}{(s-k_e^2)\sqrt{(1/(c_{bg}+v)-\zeta)(1/(c_{bg}-v)+\zeta)}}, \tag{A.1}$$

for which we seek the decomposition

$$S(\zeta) = S_+(\zeta)S_-(\zeta), \tag{A.2}$$

where both $S_+(\zeta)$ and $S_-(\zeta)$ are sectionally analytic functions.

It is convenient [following, for example, Achenbach (1973)] to express this in the form

$$\log S(\zeta) = \log(S_+(\zeta)) + \log(S_-(\zeta)). \tag{A.3}$$

Moreover, $\log S_+(\zeta)$, $\log S_-(\zeta)$ can further be expressed as

$$\log S_+(\zeta) = -\frac{1}{2\pi i}\int_{\gamma_+-i\infty}^{\gamma_++i\infty}\frac{\log S(z)}{z-\zeta}dz, \quad \mathrm{Re}(\zeta) > \gamma_+ > -\varepsilon \tag{A.4}$$

and

$$\log S_-(\zeta) = \frac{1}{2\pi i}\int_{\gamma_- - i\infty}^{\gamma_- + i\infty} \frac{\log S(z)}{z-\zeta}\,dz, \quad \mathrm{Re}(\zeta) < \gamma_- < \varepsilon. \tag{A.5}$$

Since in the present work we restrict attention to cases where $v < c_{bg}$

$$s^2 - k_e^4 = \frac{1}{c^2}(c_{bg}-v)(c_{bg}+v) > 0. \tag{A.6}$$

A polar decomposition may now be employed to advantage. The argument of function $S(\zeta)$ along branch cuts in $P_-(\zeta)$ are as follows

$$\arg S(\zeta) = \begin{cases} \pm \arctan\{\Xi(\zeta)\}, & -1/(c-v) < \mathrm{Re}(\zeta) < -\varepsilon, \quad \text{(a)} \\ \mp\dfrac{\pi}{2}, & -1/(c_{bg}-v) < \mathrm{Re}(\zeta) < -1/(c-v), \quad \text{(b)} \\ 0, & -\infty < \mathrm{Re}(\zeta) < -1/(c_{bg}-v), \quad \text{(c)} \end{cases} \tag{A.7}$$

where

$$\Xi(\zeta) \triangleq \left\{ \frac{k_e^2\sqrt{\zeta^2-\varepsilon^2}}{s\sqrt{(1/(c-v)+\zeta)(1/(c+v)-\zeta)}} \right\} \tag{A.8}$$

and the argument of $S(\zeta)$ along branch cuts in the left half space $P_+(\zeta)$ are

$$\arg S(\zeta) = \begin{cases} \pm \arctan\{\Xi(\zeta)\}, & \varepsilon < \mathrm{Re}(\zeta) < 1/(c+v), \quad \text{(a)} \\ \mp\dfrac{\pi}{2}, & 1/(c+v) < \mathrm{Re}(\zeta) < 1/(c_{bg}+v), \quad \text{(b)} \\ 0, & 1/(c_{bg}+v) < \mathrm{Re}(\zeta) < \infty. \quad \text{(c)} \end{cases} \tag{A.9}$$

Cauchy's integral theorem and [A.7(c)] and [A.9(c)] allow the rewriting of (A.4) and (A.5) as the following contour integrals

$$\log S_+(\zeta) = \frac{1}{2\pi i}\int_{\Gamma_+} \frac{\log(S)(z)}{z-\zeta}\,dz, \quad \mathrm{Re}(\zeta) > \gamma > -\varepsilon \tag{A.10}$$

and

$$\log S_-(\zeta) = \frac{1}{2\pi i}\int_{\Gamma_+} \frac{\log S(z)}{z-\zeta}\,dz, \quad \mathrm{Re}(\zeta) < \gamma < \varepsilon, \tag{A.11}$$

where integration contours $\Gamma_\pm$ are shown in Fig. A.1, and both Γ_+ and Γ_- traverse in the clockwise direction.

From Fig. A.1, one can see that there are three branch points along each integration contour; this differs from the decomposition of the Rayleigh wave function used in in-plane mode crack propagation in an elastic medium (Achenbach, 1973), for which there are only two branch points along each integration contour.

Now we proceed to evaluate the contour integral for $S_+(\zeta)$. Since $|S(\eta+i0^+)| = |S(\eta+i0^-)|$, it follows by direct (but nontrivial) application of the residue theorem that

$$\int_{\Gamma_\pm} \frac{\log|S(\zeta)|}{\eta-\zeta}\,d\eta = 0. \tag{A.12}$$

Consequently,

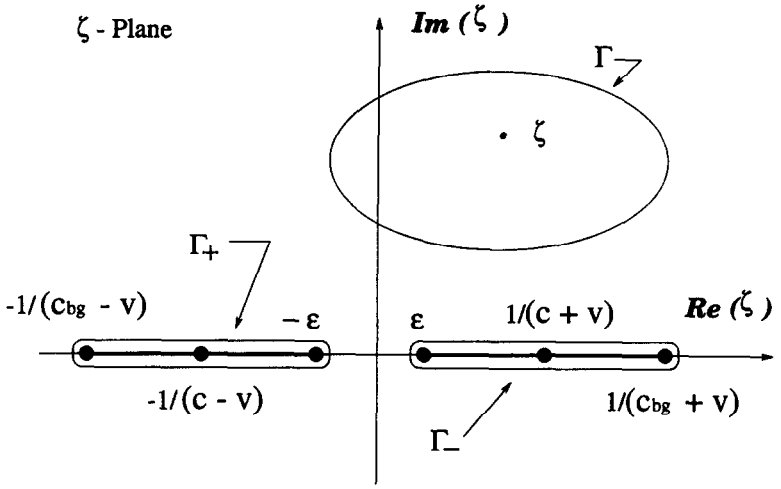

Fig. A.1. Integration contours used for product decomposition of function $S(\zeta)$.

$$\log S_+(\zeta) = \frac{1}{2}\int_{-1/(c-v)}^{-1/(c_{bg}-v)} \frac{d\eta}{\eta-\zeta} - \frac{1}{\pi}\int_{-\varepsilon}^{-1/(c-v)} \arctan\left\{\frac{k_e^2\sqrt{\eta^2-\varepsilon^2}}{s\sqrt{(1/(c-v)+\eta)(1/(c+v)-\eta)}}\right\}\frac{d\eta}{\eta-\zeta}$$

$$= \log\sqrt{\frac{1/(c_{bg}-v)+\zeta}{1/(c-v)+\zeta}} - \frac{1}{\pi}\int_{\varepsilon}^{1/(c-v)} \arctan\{\Xi(-\eta)\}\frac{d\eta}{\eta+\zeta}, \tag{A.13}$$

so that

$$S_+(\zeta) = \sqrt{\frac{1/(c_{bg}-v)+\zeta}{1/(c-v)+\zeta}}\exp\left\{-\frac{1}{\pi}\int_{\varepsilon}^{1/(c-v)} \arctan(\Xi(-\eta))\frac{d\eta}{\eta+\zeta}\right\}, \tag{A.14}$$

where

$$\Xi(\eta) \triangleq \frac{k_e^2\sqrt{\eta^2-\varepsilon^2}}{s\sqrt{(1/(c-v)+\eta)(1/(c+v)-\eta)}}. \tag{A.15}$$

Similarly,

$$S_-(\zeta) = \sqrt{\frac{1/(c_{bg}+v)-\zeta}{1/(c+v)-\zeta}}\exp\left\{-\frac{1}{\pi}\int_{\varepsilon}^{1/(c+v)} \arctan(\Xi(\eta))\frac{d\eta}{\eta-\zeta}\right\}. \tag{A.16}$$

Finally, letting $\varepsilon \to 0$ in (A.14)–(A.16) yields (82), (83) and (84).